

# Shock and Vibration Testing of an AMB Supported Energy Storage Flywheel\*

Lawrence HAWKINS\*\*, Brian MURPHY\*\*\*,  
Joseph ZIERER\*\*\* and Richard HAYES\*\*\*

Shock and vibration testing of an Active Magnetic Bearing (AMB) supported energy storage flywheel is presented. The flywheel is under development at the University of Texas-Center for Electromechanics (UT-CEM) for application in a transit bus. The flywheel is gimbal mounted to reduce the gyroscopic forces transmitted to the magnetic bearings during pitching and rolling motions of the bus. The system was placed on a hydraulic terrain simulator and driven through pitch, roll and shock motions equivalent to 150% of maximum expected bus frame values. Although the AMB control approach was originally developed specifically to ensure rotor-dynamic stability, relative rotor/housing motion was typically less than half of the backup bearing clearance under all tested conditions. Test results are presented and compared to analytical predictions for the 35 000 rpm nominal operating speed. The impact of the AMB control algorithm is discussed relative to the input forcing function.

**Key Words:** Magnetic Bearings, Flywheel Energy Storage, Magnetic Bearing Shock Response, Flywheel Battery

## 1. Introduction

UT-CEM is developing a flywheel energy storage system, or flywheel battery (FWB), for use in a power-averaging role in a hybrid electric bus. Several aspects of this project have been detailed in the literature. Hayes<sup>(1)</sup>, described the FWB design considerations and low speed testing. Hawkins<sup>(2)</sup> described the magnetic bearings, control approach and backup bearings for this system. Hawkins<sup>(3)</sup> described stator power consumption measurements with and without adaptive synchronous cancellation. Murphy<sup>(4)</sup> described the considerations of vehicle/ flywheel dynamics that led to the choices of the orientation of the FWB in the vehicle, the sizing the magnetic bearings, and the gimbal mounting of the flywheel housing to the vehicle frame.

This paper describes shock and vibration testing of the FWB, including the test facility, development of

requirements, and test results. This is the first controlled, large motion vibration test of a magnetic bearing supported flywheel battery that is large enough to be used for vehicular power averaging. The goal of this phase of the development was to design, fabricate, and perform shock and vibration testing on a complete mechanical skid for the vehicular flywheel battery. The skid integrates the FWB, a gimbal mount, gimbal axis dampers, vibration isolation, necessary auxiliary subsystems, and electrical connections into a package that is compatible with the Northrop-Grumman Advanced Technology Transit Bus (ATTB). Testing was accomplished with the flywheel skid mounted on a fully programmable four corner terrain simulator. The test plan was designed to evaluate suitability of the flywheel skid for the transit bus application and test conditions were developed to exceed the expected loads for the ATTB.

## 2. Flywheel Battery Characteristics

The flywheel rotor, which can operate at up to 40 000 rpm, spins on magnetic bearings with a nominal design capacity of 3 g in all directions. This load capacity meets the requirements imposed by typical

\* Received 27th September, 2002 (No. 02-5154)

\*\* Calnetix, Inc., 12880 Moore Street, Cerritos, California 90703, USA. E-mail: larry@calnetix.com

\*\*\* Center for Electromechanics, University of Texas, Mail Stop R7000, Austin, Texas 78712, USA

operating conditions on a transit bus, but to increase the load margin and tolerance to excessive loads, a number of additional precautions were taken. First, isolation mounts were installed between the flywheel housing and the mounting system. This attenuates the vibration transmitted to the flywheel by approximately 50% and is most important during the type of axial shock loading that occurs when hitting a pothole, curb, or other suspension bottoming event. Second, by using a gimbal mount with appropriate damping the gyroscopic forces transmitted to the magnetic bearings during pitching and rolling of the ATTB are minimized as well. These loads are associated with braking, turning or changing inclination of the bus. Finally, in the event that the magnetic bearings are overloaded, ceramic rolling element backup bearings provide a low friction interface between the rotor and stator. These would be used in the event of severe operating conditions such as: 1) passing through drainage troughs at 30 mph or greater, 2) traffic accidents, or 3) other conditions that cause the vehicle suspension to bottom.

Tables 1 and 2 summarize FWB and magnetic bearing characteristics. The tests reported here were performed on the titanium test flywheel. When testing

Table 1 Flywheel battery characteristics

	Titanium Test Flywheel	Composite Flywheel
Nom Spin Speed, rad/s (rpm)	4,190 (40,000)	3,665 (35,000)
M/G Power, kW		
Continuous	110	110
Peak	150	150
Rotor Mass, kg (lbm)	52 (114)	59 (129)
Polar Inertia, kg-m <sup>2</sup> (lbm-in <sup>2</sup> )	0.284 (969)	0.793 (2704)
Transverse Inertia, kg-m <sup>2</sup> (lbm-in <sup>2</sup> )	1.122 (3825)	1.375 (4689)
Rigid Body Ip/It	0.25	0.58
Bearing Span, m (in)	0.508 (20)	0.508 (20)

Table 2 Magnetic bearing characteristics

Bearing	Combo Bearing (Radial)	Radial Bearing	Combo Bearing (Axial)
Brg Ref Name	Brg 1	Brg 2	Thrust
Load Capacity, N (lbf)	1115 (250)	670 (150)	2230 (500)
Force Constant, N/A (lbf/A)	156 (35)	94 (21)	303 (68)
Neg. Stiffness, N/mm (lbf/in)	1751 (10,000)	963 (5500)	3502 (20,000)
Air Gap, mm (in)	0.508 (.020)	0.508 (.020)	0.508 (.020)
Max Current, A	7.1	7.1	7.4

was completed, the test flywheel was machined down and a composite flywheel pressed on, producing the higher energy capacity needed for the ATTB application. The final configuration is shown in Fig. 1.

### 3. Design Considerations for Vehicular FWB Bearing Loads

The interaction between vehicle and flywheel dynamics produces many sources of bearing loads not present in a stationary application. These loads were discussed in detail by Murphy<sup>(4)</sup>, and are summarized below.

#### 3.1 Shock loads

Shock events, such as potholes, are common occurrences in vehicles and are characterized by their brief and transient nature. Shock inputs are partially filtered by the vehicle suspension, which will have rigid body natural frequencies of a few hertz. With a

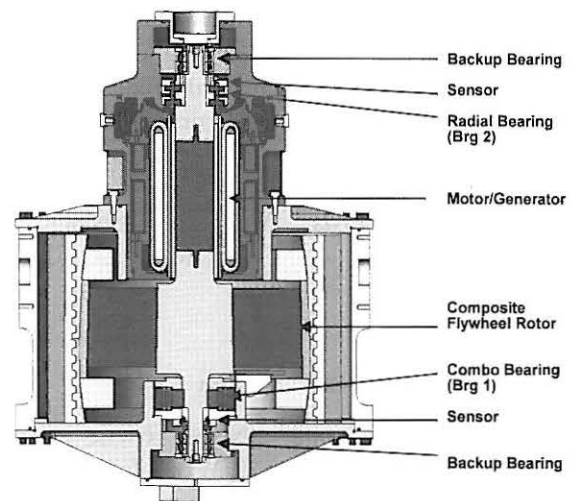


Fig. 1 Flywheel battery cross-section

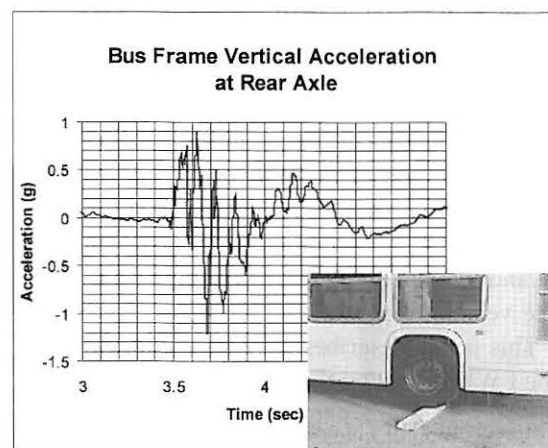


Fig. 2 Vertical acceleration measurement on ATTB rear floor, 4.5 m/s (10 mph) over 0.1 m (4.0 in) half round speed breaker

vertical spin axis, the shock loads will be born largely by the thrust bearing. Figure 2 shows vertical bus frame acceleration measurements made on a bus traveling over a 0.1 m (4 in) half round speed breaker at 4.5 m/s (10 mph). Other measurements made on an Austin, Texas city transit bus traveling around town produced similar and lower accelerations.

### 3.2 Vibration loads

Vibration is distinguished from shock in that the input and response attain steady state amplitudes that are maintained for an appreciable length of time. Sources are cobblestone roads and general road roughness. However, much of this is at higher frequencies that are generally filtered by the tires and suspension of the vehicle. The expected contribution to the bearing loads is on the order of a few tenths of a *g*.

### 3.3 Maneuvering loads

Vehicle maneuvering refers to the net rigid body motion of the vehicle, i.e. any event that changes the vehicle linear momentum such as braking, accelerating, or turning. The corresponding linear accelerations lead directly to loads on the FWB bearings; however, such loads are limited to several tenths of a *g* due to tire adhesion.

### 3.4 Gyrodynamic loads

Gyrodynamic or gyroscopic loads are produced when the flywheel spin axis is changed, usually due to maneuvering. A spinning flywheel has a relatively large angular momentum so changing its spin axis requires significant torque, which must be produced by the magnetic bearings. The required torque,  $T$  is:

$$T = I_P \omega_s \dot{\theta} \quad (1)$$

where  $I_P$  is the polar moment of inertia,  $\omega_s$  is the spin speed, and  $\dot{\theta}$  is the turning rate of the spin axis. The associated bearing loads,  $F_b$ , are approximately:

$$F_b = T/b \quad (2)$$

where  $b$  is the bearing span. When the flywheel design was initiated, the expected maximum turning rate for the bus was 6.7 degrees/sec (0.117 rad/s). For the composite flywheel, spinning at 35 000 rpm, this generates a bearing load of 669 N (150 lb) at each bearing. For the titanium test flywheel the same turning rate results in a bearing load of 274 N (54 lb) at the same 35 000 rpm spin speed.

### 3.5 Rotating mass imbalance loads

Rotating mass imbalance produces synchronous bearing loads that depend on the mass imbalance and the dynamics of the rotor/bearing system. Although the FWB rotor is well balanced the resulting bearing loads can still be a significant fraction of bearing capacity. An advantage of using magnetic bearings is that adaptive synchronous cancellation can be used to nearly eliminate bearing loading due to mass imbalance.

This has been demonstrated by many authors, and was described for this flywheel by Hawkins<sup>(3)</sup>.

### 3.6 Design considerations

Of the five loading sources mentioned above, three of them, shock, gyrodynamic, and mass imbalance, require design consideration to mitigate the loads. The shock loads are reduced by using elastomeric shock isolators between the gimbal mounting frame and the housing. The mass imbalance loads are reduced as mentioned above by using adaptive synchronous cancellation. Reducing the gyrodynamic loads require more significant efforts. First, the flywheel is oriented vertically so that yawing (turning) of the bus does not require a change in angular momentum of the flywheel, and thus no bearing reactions. During turns the vehicle will also roll (tilt) somewhat, which will still result in bearing reactions if the flywheel housing is firmly attached to the frame. Also, acceleration, deceleration, and grade changes (entering or leaving a hill) will result in pitch (front to back) motion of the vehicle, again with bearing reaction loads required to move the flywheel. An alternative to rigidly mounting the flywheel housing to the bus is to mount it in a two-axis gimbal, allowing the FWB to pitch and roll somewhat freely relative to the bus.

A two-axis gimbal was designed to support the FWB along with a mounting frame used to attach the system to the vehicle. A restoring force is required to give the flywheel a home position that is nominally vertical so that it doesn't drift too far from vertical. This restoring force is provided using gravity, by placing the rotor CG about 20 mm (0.75 in) below the gimbal pivot point. Viscous damping is provided by a rotary damper in the gimbal bearings and is adjustable to a limited extent.

## 4. Test Setup

An existing four-corner terrain simulator was modified to make it suitable for testing with the ATTB flywheel. The terrain simulator setup is shown in Fig. 3. The flywheel battery is at the top of the picture, supported in the two-axis gimbal. The gimbal frame is mounted to a support skid through elastomeric isolation mounts. The skid, which will later be mounted to the frame of the ATTB, is bolted to the table top of the terrain simulator. This system utilizes three hydraulic cylinders to simulate the pitch, roll and shock seen on a transit bus. Each of the hydraulic cylinders has a 0.254 m (10 inch) stroke and a 13 380 N (3 000 lb) capacity. A programmable controller controls table motion, and inputs and responses were measured with a Zonic signal analyzer and digital data recorder.

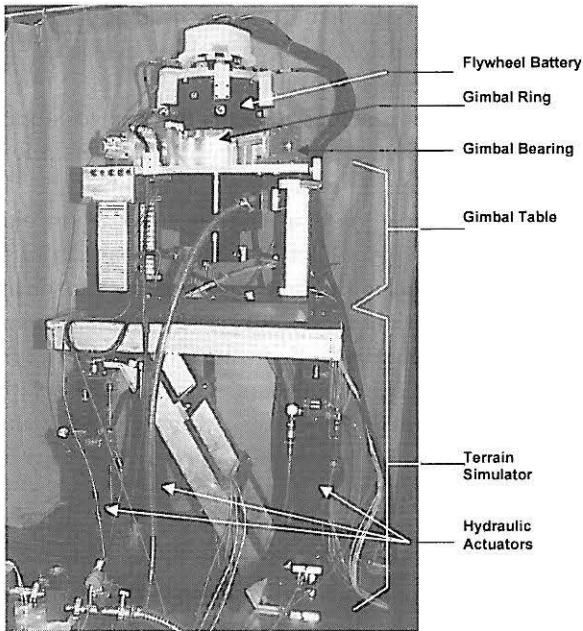


Fig. 3 Flywheel battery system mounted on terrain simulator

Liquid dielectric inclinometers were used as pitch and roll sensors on both the gimbal table and on the FWB. This type of sensor has the advantage of providing an absolute angle (an angle relative to an inertial reference frame), but they have low bandwidth compared to other available angle sensors that measure relative angles.

5. Pitch and Roll Testing

During testing the flywheel skid was mounted on the terrain simulator, and operated at speeds up to 35 000 rpm. The first test series involved pitch and roll testing to determine the effects of a variety of maneuvers on the flywheel system. The test matrix included a variety of input amplitudes and rates. The goal was to validate that the flywheel isolation, gimbal and magnetic bearings could act together to prevent back-up bearing impacts during the full range of expected motion.

The nominal input for the terrain simulator was developed based on information provided by Northrop-Grumman, the DOT White Book, and bus frame vibration measurements conducted by UT-CEM. The associated bus maneuvers are listed in Table 3. To verify operation under more aggressive conditions, the nominal amplitude and rate values were increased by 50%. These values are shown in Table 3 and represent the approximate maximum rates anticipated under all conditions. The terrain simulator applied these rates and amplitudes over a 225 second period to generate the simulated bus test route. The response of the gimbal table versus time is shown in Fig. 4,

Table 3 Simulator table input, rates and angles applied for aggressive maneuver (*P*= Pitch, *R*=Roll)

Label	Description for Nominal Maneuver	150% x Angle (deg)	150% x Rate (deg/s)
A1	Accelerate to 35 mph	P= -0.36	0.36
LC1	35 mph lane change	R= -3.0	4.5
LC2	35 mph lane change	R= 3.0	6
B1	Brake to 20 mph	P= 0.75	0.75
RT1	Gentle right turn	R= -3.0	3
H1	Dip down into culvert	P= 3.0	0.7
H2	Pitch up exiting culvt	P= -3.0	1.5
LT1	Hard left turn	R= 6.0	6
H3	7% hill at 20 mph	P= -6.0	6
LT2	Gentle left turn	R= 3.0	1.5
B2	Hard brake to stop	P= 0.75	0.75
A2	Accelerate to 20 mph	P= -0.36	3.6
RT2	Gentle right turn	R= -3.0	1.5
LC3	20 mph lane change	R= -6.0	6
A3	Accelerate to 35 mph	P= -0.36	0.36
H4	5.4% hill at 35 mph	P= -4.6	9.3
B3	Hard brake to stop	P= 0.75	0.75

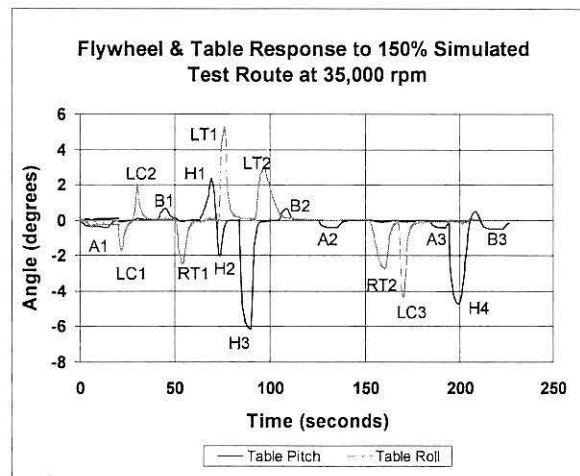


Fig. 4 Terrain simulator table motion, 150% of maximum expected inputs

along with annotations of the specific maneuvers from Table 3. The gimbal table response does not precisely match the terrain simulator input because of the low bandwidth of the pitch and roll sensors (0.5 Hz).

Figure 5 shows the displacement orbit at the non thrust end radial magnetic bearing position sensor for the entire 225 second test. The peak relative displacement is about 0.18 mm (0.007 in). This peak displacement occurred during the H4 maneuver (Table 3), an 8.1% hill (1.5 \* 5.4), which had the highest programmed slew rate of 9.3 degrees/sec. The absolute response rates of the gimbal table and the FWB during the H4 maneuver are shown in Fig. 6. The measured table angular velocity is near to the programmed value, and the flywheel response is about 65% lower at about 2.7 degrees/sec. This reduced response angle should directly result in a 65% reduc-

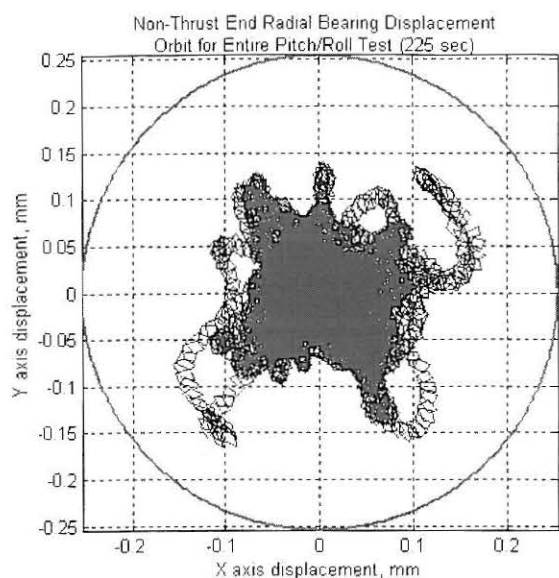


Fig. 5 Displacement orbit at non-thrust end radial position sensor throughout the test

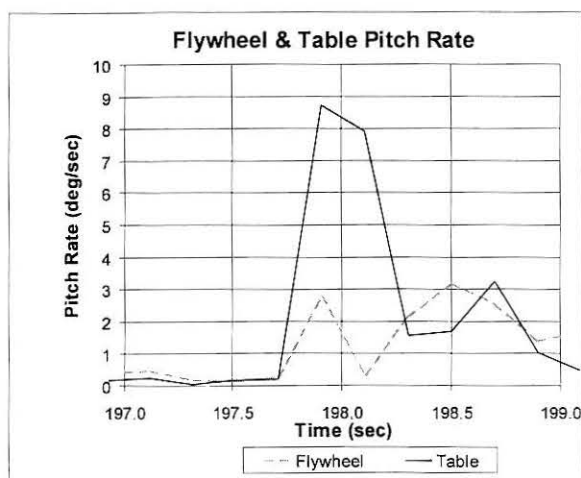


Fig. 6 Simulator table and FWB response to 150% of maximum expected inputs (deg/sec)

tion in the necessary bearing reactions during the maneuver.

A two second time slice from the H4 maneuver is shown in Fig. 7. Radial displacement,  $x$ , from the non-thrust end position sensor is shown in the upper figure and radial reaction load,  $F_b$ , at the non-thrust end bearing is shown in the lower. The loads are calculated from the measured coil current,  $I_c$ , and displacement as follows:

$$F_b = K_f I_c + K_n x \quad (3)$$

Values for the bearing force constant,  $K_f$ , and the negative stiffness,  $K_n$  are given in Table 2. Both data sets were low pass filtered at 75 Hz to take out the synchronous response. In Fig. 7, two spikes (most noticeable on displacement) occur about 0.5 seconds apart (197.7 sec and 198.2 sec). These spikes corre-

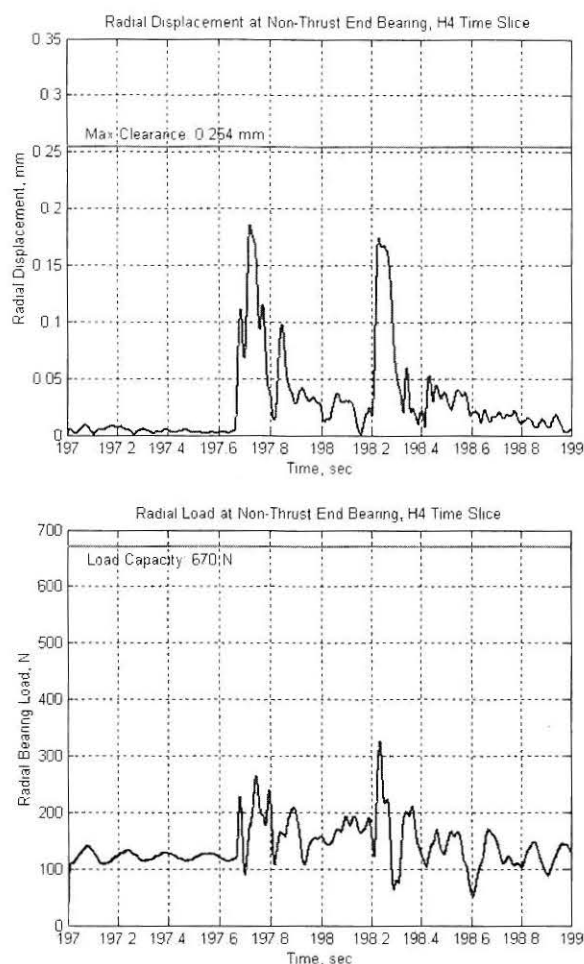


Fig. 7 Non-thrust end bearing radial position (top) and radial loads (bottom) during maneuver H4

spond to the start and end of the simulated hill. At the start of the hill the terrain simulator begins changing the pitch from 0 to 4.65 degrees over a 0.5 second period (9.3 degrees/sec). The impulse at the start and end of the maneuver causes the displacement spikes. This is an unintentional consequence of the test apparatus dynamics; however, similar impulses might be expected to occur along with many of the real world events in Table 3. The response during the period where the pitch is being steadily changed does not show a significant change in displacement, but does show a load increase of approximately 75 to 100 N. Per Eq.(2), the load would be approximately 333 N (75 lbf) if the flywheel were not gimbaled. This correlates reasonably well with the angle rate difference in Fig. 6.

## 6. Shock Testing

The terrain simulator was also used to perform vertical shock testing, to determine the vertical acceleration that could be tolerated before impacting the backup bearings. Figure 8 shows the results from one

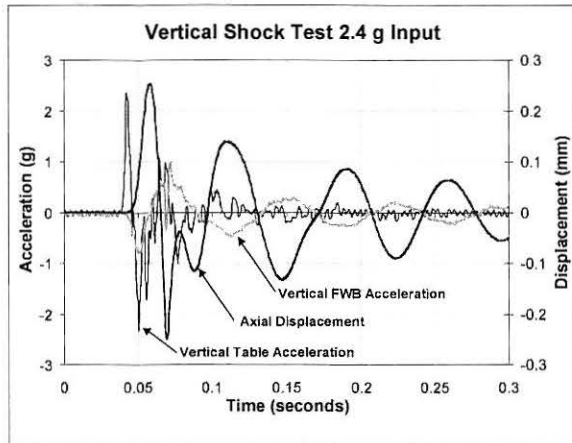


Fig. 8 Axial shock test results showing 2.4 g input, FWB response, and relative rot/hsg displacement

of the tests. The table acceleration, FWB acceleration, and relative rotor/housing displacement are shown in the figure. The simulator input acceleration is 2.4 g at 100 Hz, the highest input level that could be used without the rotor hitting the backup bearings. The associated FWB response was about 0.8 g (65% reduction) at the 15 Hz natural frequency of the FWB mass on the isolator stiffness of 2.2 MN/m (12 500 lbf/in). Relative rotor/housing displacement is just below the backup bearing clearance of 0.25 mm (0.010 in).

Although the 2.4 g input is well below the acceleration level measured in an actual bus (Fig. 2), it is desirable to consider improvements and to consider the influence of the higher system mass planned for the composite flywheel. A simple 3 degree-of-freedom model was created for this purpose. The simulator table, FWB housing and FWB rotor masses were connected by discrete stiffness and damping elements to represent the isolators and axial magnetic bearing. The results, shown in Fig. 9, provide a reasonable match to the data from Fig. 8, although the predicted acceleration of the FWB housing is somewhat low. The two biggest sources of error in the model are: 1) the simplicity of the model compared to the test system, and 2) the stiffness and damping of the isolators, which varies with preload. The model is adequate to serve its intended purpose of trading-off potential system changes. Since the critical parameter for the trade study is axial displacement, the isolator stiffness and damping were increased by 20% from nominal to match the predicted displacement to the tested value. The model was then used to predict relative rotor housing response due to a 2.4 g input with three variations: 1) increase net magnetic bearing stiffness by 50% (15% increase in compensator gain), increase FWB housing and rotor mass to correspond to the values expected for the composite sys-

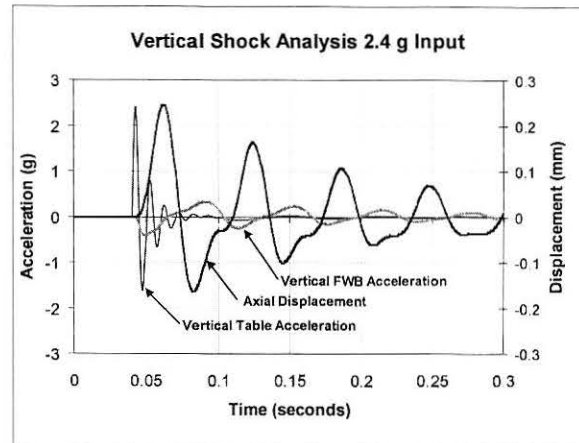


Fig. 9 Three dof analysis of axial shock test showing input, FWB response, and rel. displacement

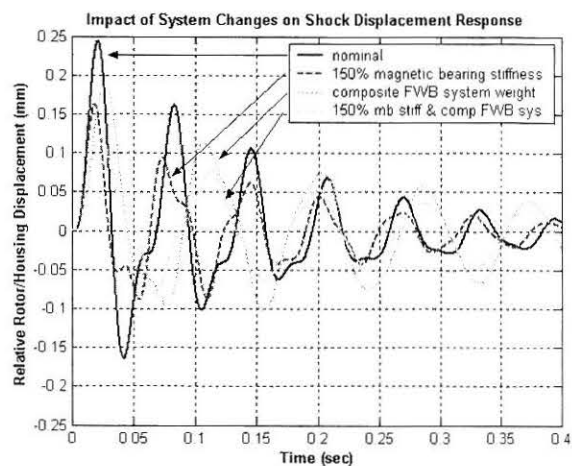


Fig. 10 Predicted displacement response for various system changes

tem, and 3) increase both magnetic bearing stiffness and FWB housing and rotor mass. The results from these three variations are compared to the nominal model in Fig. 10. Increasing the stiffness alone attenuates the peak response by 35%, increasing the mass reduced the peak response by about 20%, and the combination of the two decreases the peak response by over 50%.

## 7. Conclusions

The reported testing has verified the suitability of the flywheel battery skid system for field testing in a transit bus. The gimbal support reduced the flywheel bearing loads by about 65%. The shock isolators reduced the transmitted axial shock by 65%. Most importantly, the control of the flywheel on the magnetic bearings is maintained for shock and vibration levels well in excess of the values that are expected in the transit bus.

### Acknowledgements

This work was completed under funding provided by the US Dept. of Trans. (DOT) through the Southern Coalition for Advanced Transportation (SCAT) and by the Houston Metropolitan Transit Authority (HMTA).

### References

- (1) Hayes, R.J., Kajs, J.P., Thompson, R.C. and Beno, J.H., Design and Testing of a Flywheel Battery for a Transit Bus, SAE 01-1159, (1999).
  - (2) Hawkins, L.A., Murphy, B.T. and Kajs, J.P., Analysis and Testing of a Magnetic Bearing Energy Storage Flywheel with Gain-Scheduled, MIMO Control, ASME 2000-GT-405, Presented at ASME IGTI Conference, Munich, Germany, May 8-11, (2000).
  - (3) Hawkins, L.A. and Flynn, M., Influence of Control Strategy on Measured Actuator Power Consumption in an Energy Storage Flywheel with Magnetic Bearings, Proc. of the 6th Intl. Symp. on Magnetic Suspension Tech., Turin, Italy, October 7-11, (2001).
  - (4) Murphy, B.T., Beno, J.H. and Bresie, D.A., Bearing Loads in a Vehicular Flywheel Battery, PR-224, SAE Int. Congress and Exp., Detroit, Michigan, USA, February, 24-27, (1997).
-

# Information for Authors

## 1. Originality

Papers submitted must be original, and previously unpublished.

## 2. Language and Units

The language of the Journal is English and the units used are SI.

## 3. Receiving Date

The date of receipt of the manuscript is the date of its arrival at the society's office.

## 4. Acceptance

Acceptance or rejection of submitted papers will be based on and determined by the refereeing standards of the Journal's editorial committee.

## 5. Responsibility of Contents

The responsibility for the contents of published articles rests solely with the authors and not the society.

## 6. Page Charge

A charge of ¥10,000 (or equivalent US \$) per printed page will be invoiced to the author or the author's designated institution. 50 reprints will be provided to the lead author following publication and receipt of payment.

## 7. Length of Paper

The manuscript should be prepared in 6500-9000 words including figures and tables (approximately 6-8 pages in printed form).

## 8. Manuscript

Please type manuscripts using A4 (21 cm × 30 cm) or 8.5 inch × 11 inch sheets.

One typed page should contain 26 lines with approximately 65 characters per line. When this guideline is followed, three type-written pages will make up one printed page.

Sample Layout :

1st page : Title, names of authors, affiliation and address, key words and mailing address

2nd page : Abstract of less than 150 words

3rd page and following pages : Text

The text should be arranged in the following manner :

Introduction, Materials and Methods, Results, Discussions, Acknowledgments, References, Figure Legends and Tables.

## 9. Style

Use short paragraphs wherever possible. Express ideas clearly, and avoid using jargon. Abbreviations should be explained in the text. If many abbreviations are used, a table of abbreviations should be included.

## 10. Mathematical Expressions

All mathematical expressions should be numbered in parentheses and typed. Symbols not available on the typewriter should be carefully inserted.

## 11. Figures

Drawings for figures must be submitted on separate sheets, drawn in black India ink and carefully lettered and also the lettering be proportionate so that it does not become illegible or unclear after reduction by the printers. The appropriate placement of each figure in the text should be indicated in the margin and equations be contained to one column in width.

## 12. References

References lists should be typed, double-spaced, on a separate sheet following this example :

- (1) Fuller, E.W. and Stoessel, R.F., Factory Automation, Mech. Eng., Vol. 109, No. 3 (1987), p. 42-45.
- (2) Akasaka, T., Shibuya, K. and Shinjuku, T., Automotive Electronics, Trans. Jpn. Soc. Mech. Eng., (in Japanese), Vol. 53, No. 785, A (1987), p. 340-346.

## 13. Copyright

Copyright of the materials published in the Journal belongs to the JSME.

## 14. Submission of Manuscripts

Please send three copies of your manuscript to :

JSME International Journal Editorial Board  
Shinanomachi-Rengakan Building, Shinanomachi 35,  
Shinjuku-ku, Tokyo 160-0016, Japan